LHC discovery potential of the lightest NMSSM Higgs in $h \to a_a \to \mu\mu\mu\mu$ channel

Alexander Belyaev,[1,2] Jim Pivarski,[3] Alexei Safonov,[3] and Sergey Senkin[3]

[1] *School of Physics & Astronomy, University of Southampton, Highfield, Southampton SO17 1BJ, UK*

[2] *Particle Physics Department, Rutherford Appleton Laboratory, Chilton, Didcot, Oxon OX11 0QX, UK*

[3] *Physics Department, Texas A&M University*

(Dated: September 5, 2009)

We explore the potential of Large Hadron Collider to observe $h_1 \to a_1 a_1 \to 4\mu$ signal from the lightest lightest scalar Higgs boson (h_1) decaying into two lightest pseudoscalar Higgs bosons(a_1) followed by their decays into 4 muons within the Next-to-Minimal Supersymmetric Standard Model (NMSSM). The signature under study allows to cover the NMSSM parameter space with M_{a_1} below 3.5 GeV and large $Br(h_1 \to a_1 a_1)$ which has not been studied previously. In case of such a scenario, the suggested strategy of the observation of 4μ signal with the respective background suppression would provide a unique way to discover the lightest scalar NMSSM Higgs boson.

PACS numbers: 13.38.Dg 13.38.Qk

Contents

I. INTRODUCTION

The next-to-minimal supersymmetric standard model (NMSSM) [1–13] is extended by one singlet superfield in addition to the particle content of the Minimal Supersymmetric Standard Model (MSSM) and due to this design has several new attractive features as compared to MSSM. First of all, NMSSM elegantly solves so called μ-problem [14]: the scale of the μ-parameter is automatically generated at the electroweak or SUSY scale when the singlet Higgs acquires a vacuum expectation value. On the other hand NMSSM can solve fine-tuning and little hierarchy problems of MSSM [15]. The upper mass limit on the lightest CP-even Higgs boson in NMSSM is larger than in MSSM and since more parameter space survives LEP II bounds from the Higgs search, NMSSM is less fine-tuned. On the other hand there is additional mechanism for the reduction of fine-tuning since LEP II bounds from the Higgs search can be partly avoided if the branching of $h_1 \rightarrow a_1 a_1$ decay is significant (h_1 and a_1 stands for the lightest CP-even and CP-odd Higgs bosons respectively). This decay channel of h_1 diminishes the branching ratios for conventional modes used in direct Higgs searches and largely softens direct Higgs boson mass limits from LEP.

One should stress that due to the extended scalar sector (in comparison to MSSM) NMSSM offers richer Higgs collider phenomenology [16–24] as well as richer cosmological Dark Matter implications related to the presence of the fifth neutralino ("singlino"), relic density for which can be achieved to be correct one [25].

The collider phenomenology of the Higgs sector of the NMSSM is very interesting in several aspects, therefore a short historical introduction is in order. In [17] the first attempt to establish 'no-lose' theorem for NMSSM has been done. This theorem states that LHC has a potential to discover at least one NMSSM Higgs boson in the conventional mode given that Higgs-to-Higgs decay modes are not important. However the point is that Higgs-to-Higgs decay modes can be important as has been shown and studied later on in analysis devoted to re-establishing of 'no-lose' theorem [18–24] for the case when $h_1 \rightarrow a_1 a_1$ decay is significant and a_1 is light. So far, the case of the lightest a_1 was explored for m_{a_1} below $2b$-quark threshold but above 2τ one, $2m_\tau < m_{a_1} < 2m_b$, establishing the scope of the 4τ channel in Higgs-strahlung and Vector Boson Fusion for the NMSSM No-Lose Theorem at the LHC [24]. Theses analysis require a substantial integrated luminosity (10-100 fb^{-1}) and quite challenging analysis in the technical sense.

In this paper we explore the mass region of a_1 with the mass below 2μ threshold: $m_{a_1} < 2m_\mu$. In this case, which has not been studied previously, we explore $h_1 \to a_1 a_1 \to \mu\mu\mu\mu$ signature. Unlike searches for 4τ signature, the measurement of invariant mass of muon pair provides a direct estimate of m_{a_1} which defines a clear set of the kinematical cuts for the background suppression. Further, this channel is essentially free of backgrounds and therefore allows to use direct gluon fusion production combined with $b\bar{b}$ fusion production instead of subdominant vector boson fusion or associate Higgs production processes used in case of 4τ signature to to suppress large QCD backgrounds.

We demonstrate that the analysis in the four muon mode has excellent sensitivity for Lightest CP-even NMSSM Higgs boson and can be performed with just a handful of first CMS data and requires very little in terms of detector performance except reasonably robust tracking for muons and well functioning muon system. To make this a realistic analysis, we use parameters of the CMS experiment in designing selections and estimating background contributions.

The rest of the paper is organized as follows. In Section II we study the NMSSM parameters space for which $m_{a_1} < 2m_\mu$ case of our study is realized. In Section III we perform signal versus background analysis and present our final results in Section IV. In Section V we draw our conclusions.

II. NMSSM PARAMETER SPACE AND SIGNAL PRODUCTION RATES

A. The model and the parameter space for the light a_1 scenario

In our study we consider the simplest version of NMSSM [1–12], where $\mu\widehat{H_1}\widehat{H_2}$ term of the MSSM superpotential is replaced by

$$\lambda\widehat{S}\widehat{H}_1\widehat{H}_2 + \frac{\kappa}{3}\widehat{S}^3 \tag{1}$$

which makes superpotential scale invariant. In addition, we have five soft braking terms in general, "non-universal" case:

$$m^2_{H_1}H_1^2 + m^2_{H_2}H_2^2 + m^2_S S^2 + \lambda A_\lambda H_1 H_2 S + \frac{\kappa}{3}A_\kappa S^3. \tag{2}$$

In the above equations the tilded capital letters denote superfield while non-tilded ones stand for the scalar component of the respective superfield.

Soft breaking parameters $m^2_{H_1}$, $m^2_{H_2}$ and m^2_S from Eq. 2 can be traded for M_Z, the ratio of the doublet Higgs vacuum expectation values (VEVs) $\tan\beta$, and $\mu = \lambda\langle S\rangle$ (where $\langle S\rangle$ denotes the VEV of the singlet Higgs field) through the three minimization equations of the Higgs potential. Therefore, assuming that the Higgs sector is CP conserving, the NMSSM Higgs sector at the Electro-Weak (EW) scale is uniquely defined by fourteen parameters: $\tan\beta$, the trilinear couplings in the superpotential λ and κ, the corresponding soft SUSY breaking parameters A_λ and A_κ, the effective μ parameter $\mu = \lambda\langle S\rangle$, the gaugino mass parameters M_1, M_2 and M_3, the squark and slepton trilinear couplings A_t, A_b and A_τ, and the squark and slepton mass parameters M_{f_L} and M_{f_R}. For simplicity, we assume here the universality within 3 generations for the last two parameters.

In the following we study the NMSSM parameter space, defined in terms of the above inputs, that survive theoretical and experimental constraints except direct searches by LEP [ref] and the Tevatron [ref], which we show explicitly in our results **(not yet for the LEP result)**. We make use of NMSSMTools package [26–28] to scan the NMSSM parameter space and to identify the region of our interest, where $B_{h\to aa\to 4\mu}$ is dominant over the MSSM (conventional) Higgs boson decay modes $B_{h\to WW^*,\, b\bar{b},\, \tau^+\tau^-}$.

We scanned the NMSSM parameter space uniformly in the following:

- $100\ \text{GeV} < \mu < 1000\ \text{GeV}$
- $0 < \lambda < 1$
- $1.5 < \tan\beta < 50$
- $-1\ \text{TeV} < A_\lambda < 5\ \text{TeV}$
- $0 < \mu\kappa/\lambda < 120\ \text{GeV}$
- $-3\ \text{GeV} < A_\kappa - (30\ \text{GeV})\lambda^2 < 0.1\ \text{GeV}$.

The first four ranges broadly cover all models that survive theoretical and experimental constraints (except the upper limits on μ and $\tan\beta$). The fifth, effectively a non-uniform metric and boundary for κ, was chosen because it is closely related to properties of the CP-even Higgs sector. The last, a parabolic selection in the A_κ-λ plane, is roughly uniform in a_1 mass, selecting the low m_a region. This puts a very narrow constraint on A_κ, from -3 to about 14 GeV. The upper limit on this parabolic selection, 0.1 GeV, is not restrictive

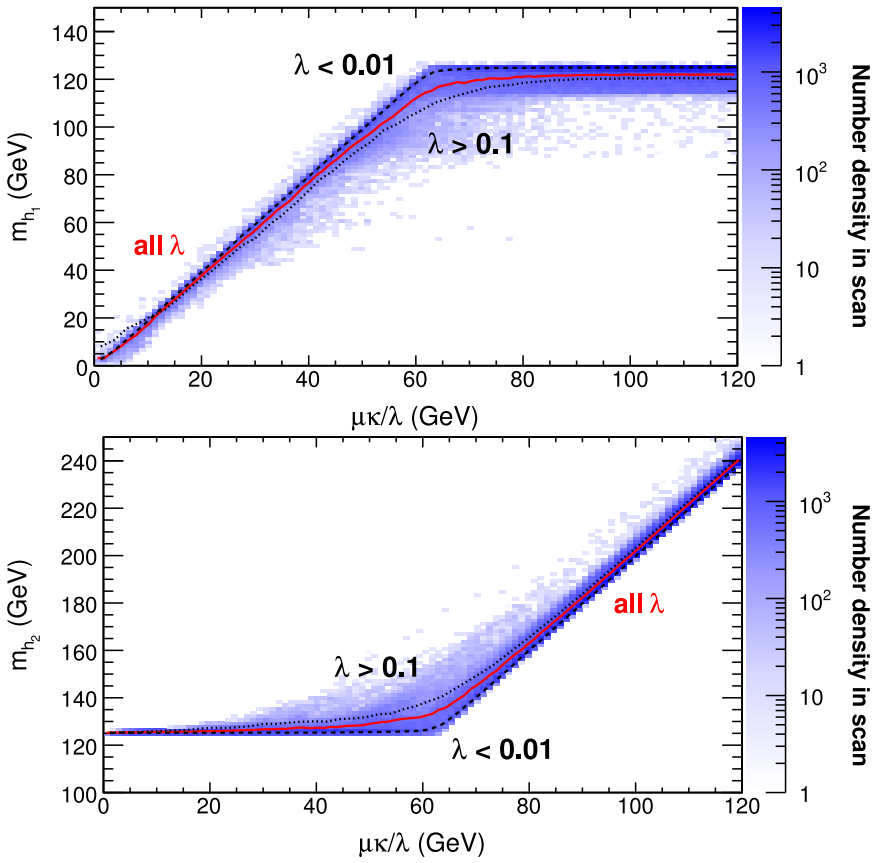

FIG. 1: Lightest (h_1, top) and second-lightest (h_2, bottom) CP-even Higgs masses as a function of $\mu\kappa/\lambda$ and λ. The density of generated points surviving constraints is shown in the color scale, with the lines being the average value as a function of $\mu\kappa/\lambda$. The central red line is an average over all points, the dashed line requires $\lambda < 0.01$ and the dotted line requires $\lambda > 0.1$.

because the physical region ends at 0 GeV. The phenomenology of $pp \to h_1 \to a_1 a_1 \to 4\mu$ is determined almost exclusively by the $\mu\kappa/\lambda$ ratio, λ, and A_κ. Varying $\tan\beta$ and A_λ has negligible effect on all of the following.

Several properties follow almost directly from $\mu\kappa/\lambda$, the simplest being the CP-even Higgs boson mass. One of the two lightest scalars, h_1 and h_2, has a mass which is nearly equal to $2\mu\kappa/\lambda$; the other has a constant value at 125 GeV and plays the role of the Standard Model Higgs. This relationship and a small variation with λ are shown in Fig. 1.

The mass of the lightest CP-odd Higgs has a simple distribution in the A_κ-λ plane, shown in Fig. 2. In this space, the region $A_\kappa > (30\text{ GeV})\lambda^2$ is unphysical (no sampled points in NMSSMTools survive). The smallest m_a values can be found along the edge of this unphysical region, with m_a growing with distance. Only a_1 bosons below the $2m_\tau$

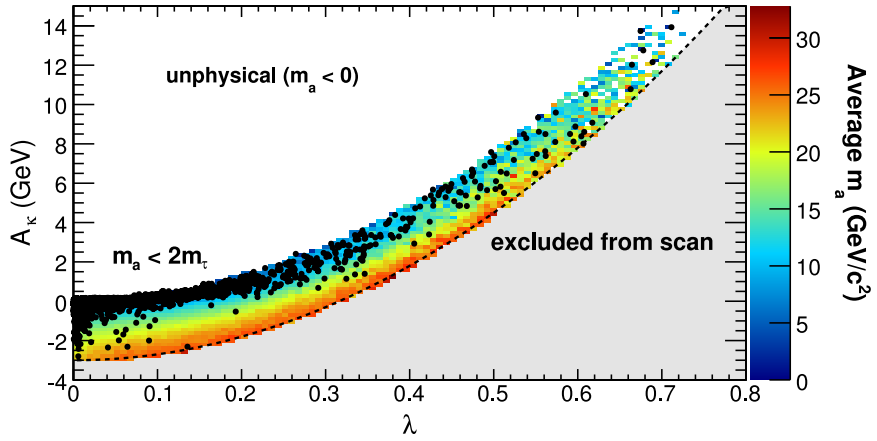

FIG. 2: Mass of the CP-odd Higgs (m_a) as a function of A_κ and λ. The color scale is the average m_a in each bin. The grey region below the dashed line is excluded from our scan by construction, but the region above the sampled points is unphysical. Filled circles are models with $m_a < 2m_\tau$.

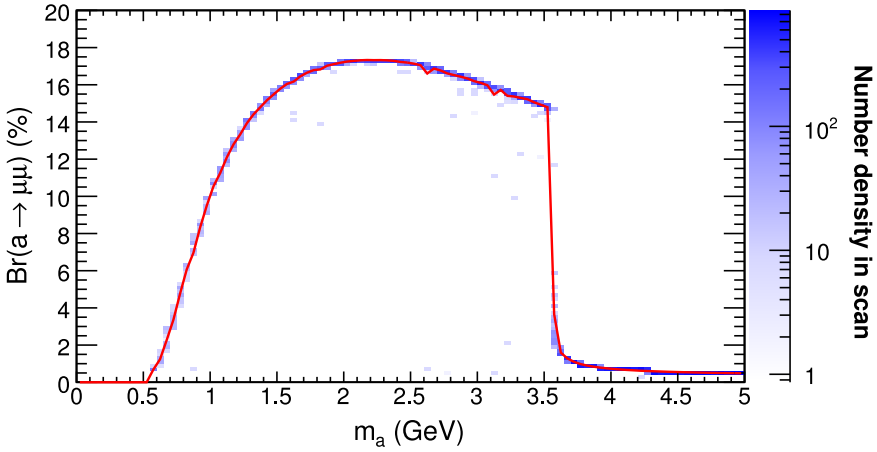

FIG. 3: The mass of a_1 and its branching fraction to muons for generated models. The red line is the average as a function of m_a, demonstrating that the branching fraction is nearly a strict function of mass. The threshold at 3.55 GeV is $2m_\tau$.

theshold decay significantly into muon pairs (Fig. 3), so we are interested in points close to the edge. The parabolic cut described above allows us to sample that region uniformly.

For a quantity which is more simply related to m_a, we can unfold the parabolic shape in Fig. 2 and consider $A_\kappa - (30\text{ GeV})\lambda^2$ the model parameter. Figure 4 shows that m_a is also a function of $\mu\kappa/\lambda$. For most (80%) of the sampled points,

$$\left[A_\kappa - (30\text{ GeV})\lambda^2\right] \cdot \frac{\mu\kappa}{\lambda} \approx -(0.58\, m_a)^2 \tag{3}$$

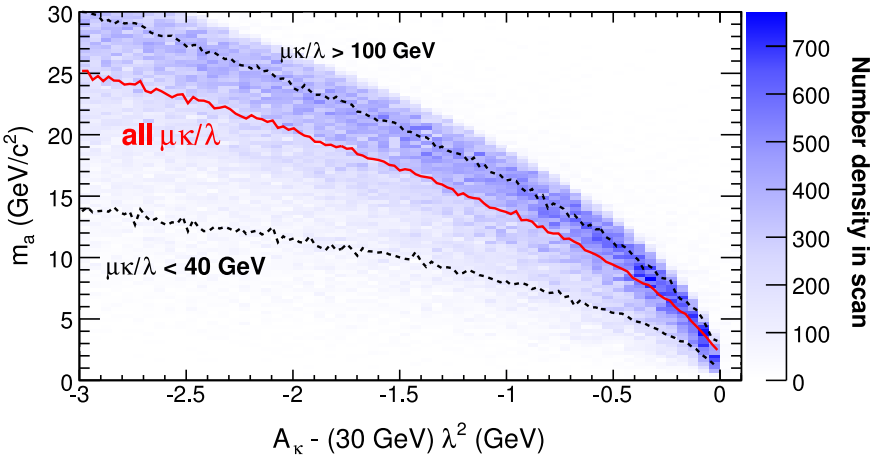

FIG. 4: Mass of the CP-odd Higgs (m_a) versus $A_\kappa - (30\text{ GeV})\lambda^2$, which is the parabolic curve of Fig. 2 unfolded. The residual variation is due to $\mu\kappa/\lambda$, with the upper edge being an artifact of our $\mu\kappa/\lambda < 120$ GeV scan boundary.

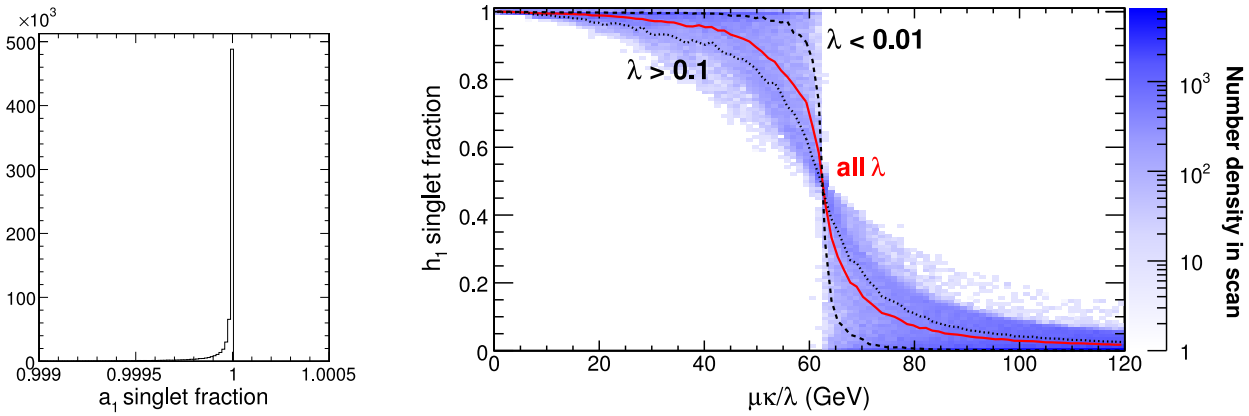

FIG. 5: Singlet fraction of h_1 and a_1. The singlet fraction of a_1 is nearly constant and approximately 1.0, while the singlet fraction of h_1 depends on $\mu\kappa/\lambda$ and λ.

with at least 10% accuracy.

The couplings of h_1 and a_1 are determined by their singlet fraction. The CP-odd Higgs is always highly singlet ($|zzz - 1| \lesssim 10^{-5}$), but the singlet fraction of h_1 depends on $\mu\kappa/\lambda$ and λ (Fig. 5). **What is zzz? These values are $SCOMP(1,3)^2$ and $PCOMP(1,2)^2$; what symbol will we use for this in the text?** The threshold just above 60 GeV is the point where h_1 takes the role of the Standard Model Higgs and becomes a doublet. Large values of λ soften this threshold.

The nearly-singlet a_1 is only weakly coupled to Standard Model particles: it decays

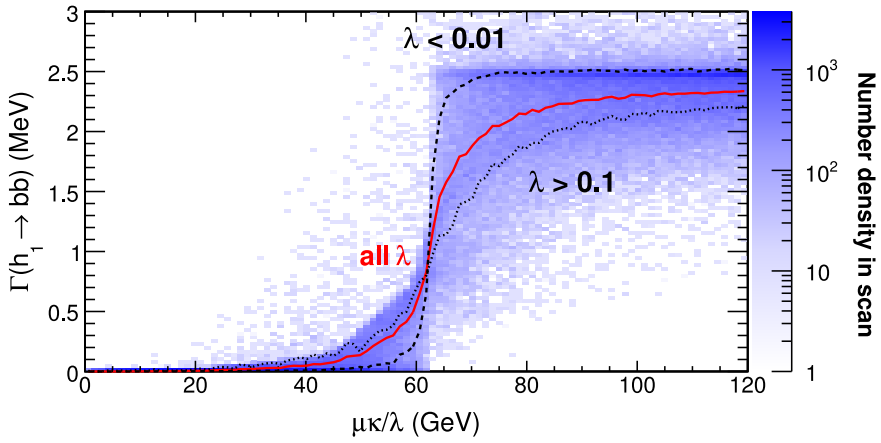

FIG. 6: Partial width of $h_1 \to b\bar{b}$ as a function of $\mu\kappa/\lambda$ and λ.

primarily into Standard Model fermion pairs only because of kinematics. The couplings of h_1 to Standard Model particles depend on its singlet fraction, and consequently $\mu\kappa/\lambda$ and λ. As an illustration, consider the conventional Higgs decay to $b\bar{b}$: in the NMSSM, the partial width for this decay is a strong function of $\mu\kappa/\lambda$, growing rapidly above 60 GeV (see Fig. 6). Again, large values of λ soften the dependence. We will find the same to be true for production cross-sections.

The distribution of $h_1 \to a_1 a_1$ partial widths and branching fractions is more complicated. Figure 7) presents both quantities in the $\mu\kappa/\lambda$, λ plane. There are two regions with high branching fraction: a low $\mu\kappa/\lambda$ region where competing Standard Model contributions are small, and a high λ region where the $h_1 \to a_1 a_1$ rate is high.

B. Production rates

We calculate the $pp \to h_1$ production cross-section from two contributions: $gg \to h_1$ and $b\bar{b} \to h_1$. In each case, we compute the standard model $pp \to H_{SM}$ using next-to-leading order (NLO) tools, then correct by a factor relating Standard Model cross-sections to NMSSM, thereby obtaining NLO cross-sections in the NMSSM.

For $gg \to H_{SM}$, we used the HIGLU v2.102 package [31]. The ratio $\sigma(gg \to h_1)/\sigma(gg \to H_{SM})$ is equal to the ratio of partial decay widths $\Gamma(h_1 \to gg)/\Gamma(H_{SM} \to gg)$, so one finds

$$\sigma(gg \to h_1) = \sigma(gg \to H_{SM}) \frac{\Gamma(h_1 \to gg)}{\Gamma(H_{SM} \to gg)} = \sigma(gg \to H_{SM}) \frac{Br(h_1 \to gg)\Gamma^{tot}(h_1)}{\Gamma(H_{SM} \to gg)}. \qquad (4)$$

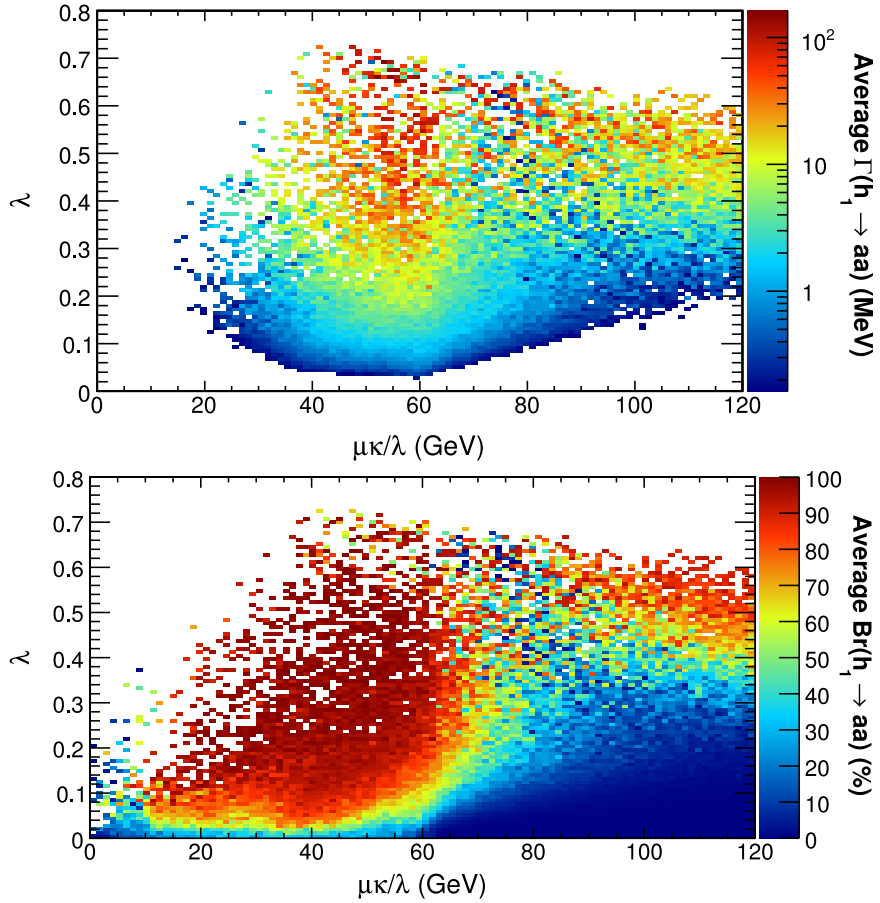

FIG. 7: The partial width (top) and branching fraction (bottom) of $h_1 \to a_1 a_1$ in the λ, $\mu\kappa/\lambda$ plane.

Therefore we have all components to evaluate $\sigma(gg \to h_1)$: we use $\sigma(gg \to H_{SM})$ and $\Gamma(H_{SM} \to gg)$ calculated using HIGLU at NLO, while $Br(h_1 \to gg)$ and $\Gamma^{tot}(h_1)$ we obtain using NMSSMTools.

For $b\bar{b} \to h_1$, we used the $b\bar{b} \to H_{SM}$ program developed in [33] and lately used also in [34] where the QCD-improved (running) Yukawa couplings have been used. Then using $Y_{bbh_1}/Y_{bbH_{SM}}$ ratio of Yukawa couplings calculated in NMSSMtools, one finds:

$$\sigma(b\bar{b} \to h_1) = \sigma(b\bar{b} \to H_{SM}) \left(\frac{Y_{bbh_1}}{Y_{bbH_{SM}}} \right)^2 \tag{5}$$

For the evaluation of production cross sections, CTEQ6M set for parton density function set was used.

The gg and $b\bar{b}$ contributions to the cross-section are presented in Fig. 8, with their sum. The cross-section depends on $\mu\kappa/\lambda$ and λ in a way which is similar to the h_1 singlet fraction

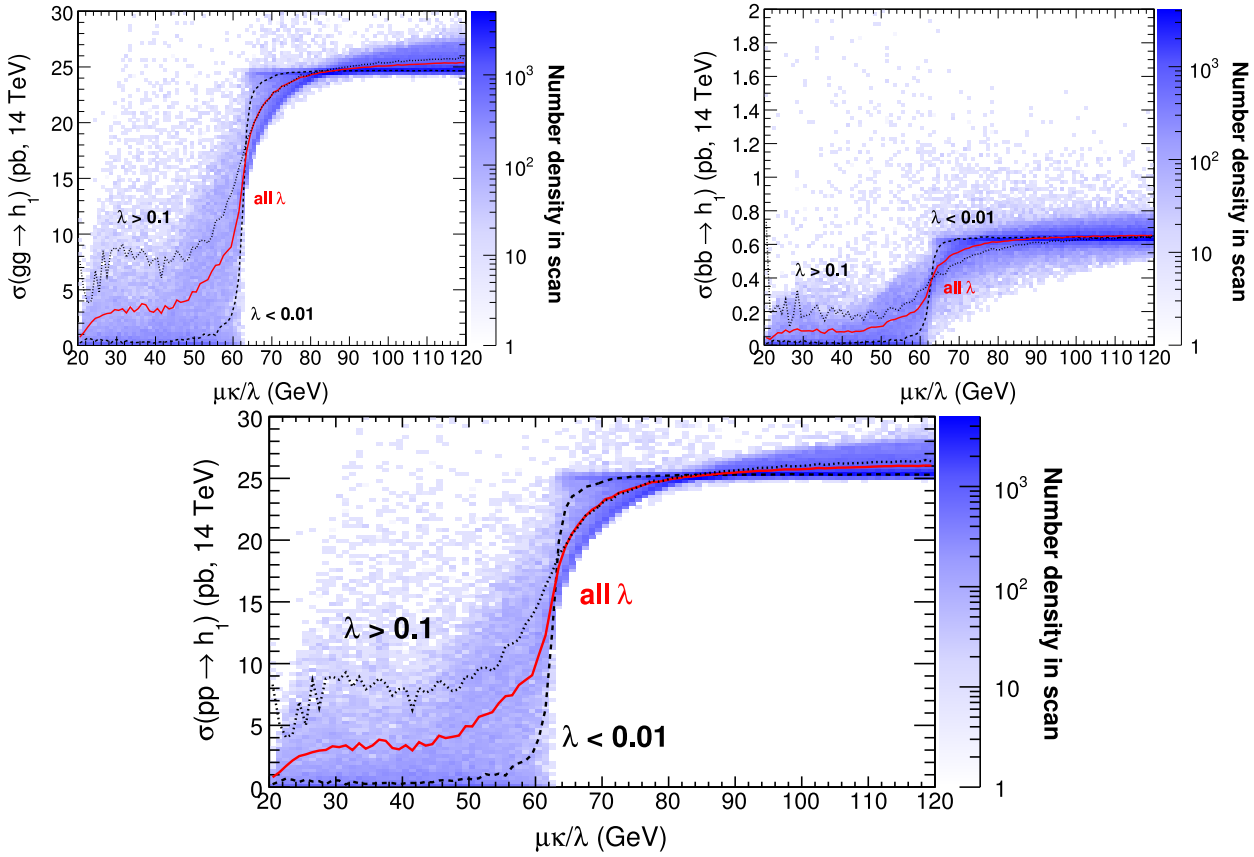

FIG. 8: Production cross-section of h_1 as a function of $\mu\kappa/\lambda$ and λ. Top-left: gg contribution only. Top-right: gg contribution only. Bottom: total cross-section.

(Fig. 5) and Standard Model decay widths (Fig. 6).

To predict event rates at colliders, we must assemble the branching fractions for each step in the decay chain, $B_{h_1\to a_1a_1}$ and $B_{a_1\to\mu\mu}$, and the production cross-section $\sigma(pp\to h_1)$ into an effective cross-section $\sigma(pp\to h_1\to a_1a_1\to 4\mu)$. Figures 9, 10, and 11 present the total branching fraction and effective cross-section in the $A_\kappa - (30\text{ GeV})\lambda^2$, $\mu\kappa/\lambda$ and λ, $\mu\kappa/\lambda$ planes. Models with total branching fractions higher than 1% and cross-sections higher than 100 fb are highlighted with points.

C. Excluded regions of parameter space

Even though the four-muon signal rates from NMSSM are not high, due to relatively low expected backgrounds the signature of our interest would allow us to exclude significant portion of NMSSM parameter space even at low integrated luminosities as we present below.

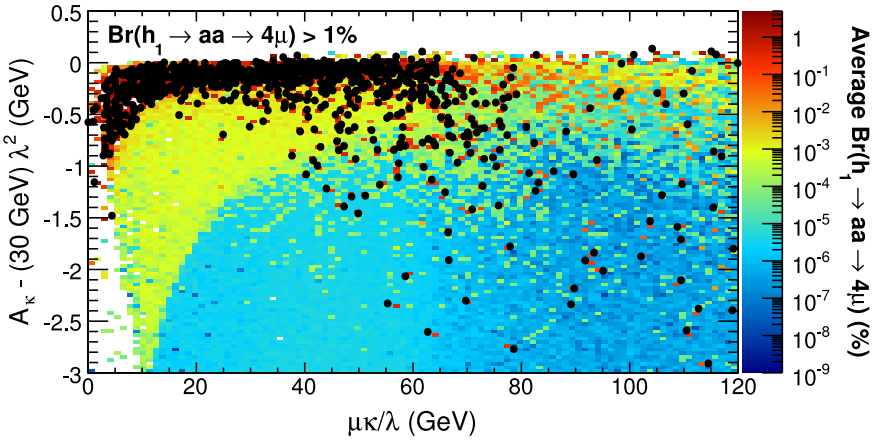

FIG. 9: Total branching fraction $B_{h_1 \to a_1 a_1 \to 4\mu}$ in the $A_\kappa - (30\text{ GeV})\lambda^2$, $\mu\kappa/\lambda$ plane. Filled circles represent a subsample of models with branching fraction above 1%.

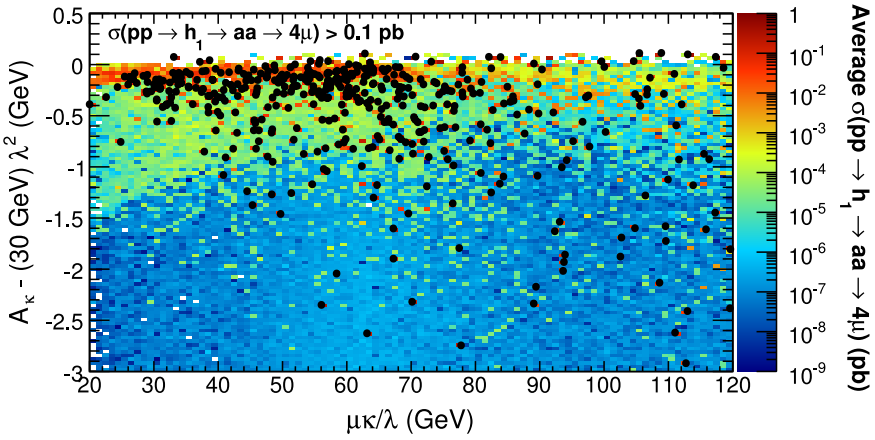

FIG. 10: Effective cross-section $\sigma(pp \to h_1 \to a_1 a_1 \to 4\mu)$ in the $A_\kappa - (30\text{ GeV})\lambda^2$, $\mu\kappa/\lambda$ plane. Filled circles represent a subsample of models with cross-sections greater than 0.1 pb.

The parameter space accessible at the LHC at low and later on at high luminosity regime is quite unique since it can not be excluded by present low-energy experiments on rare B-meson decays since, as we have found the singlet component of the lightest CP-odd Higgs boson, a_1, is extremely close to unity [ref still needed]. This forbids $\Upsilon \to \gamma a_1$ well beyond the experimental bounds.

LEP exclusion hasn't been included yet, because we don't know if NMSSMTools is doing the right thing.

Figure 12 illustrates the reach of the Tevatron and LHC (assuming an integrated luminosity $\mathcal{L}$ of 100 pb^{-1} and collision energy of 14 TeV) in the branching fraction, production

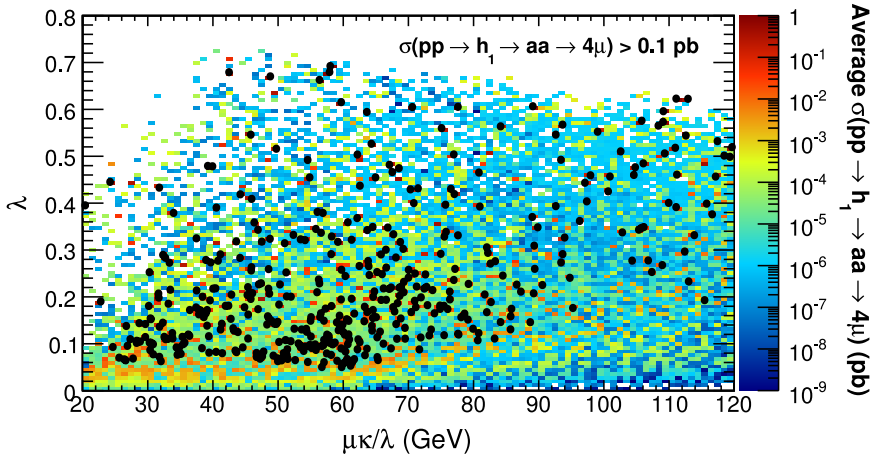

FIG. 11: Effective cross-section $\sigma(pp{\to}h_1{\to}a_1a_1{\to}4\mu)$ in the λ, $\mu\kappa/\lambda$ plane. Filled circles represent a subsample of models with cross-sections greater than 0.1 pb.

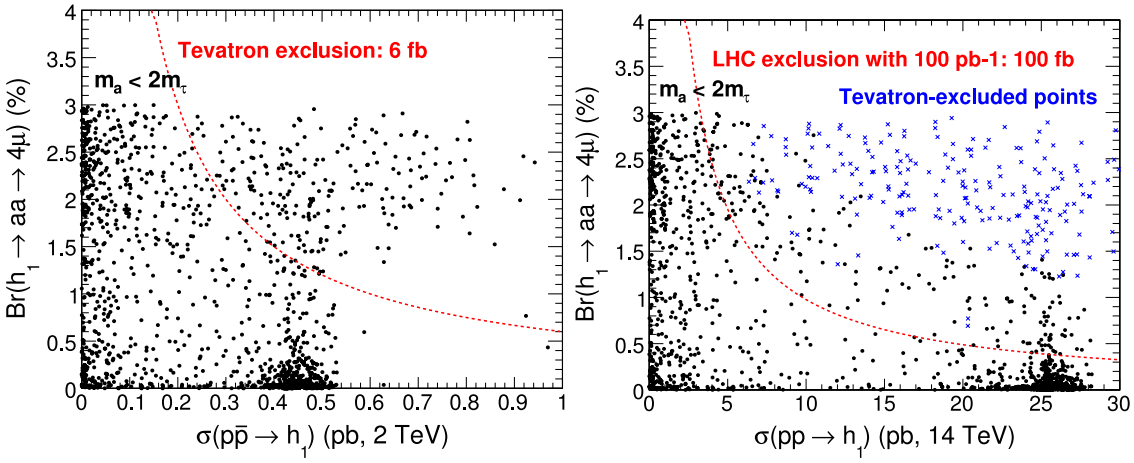

FIG. 12: Exclusion from the Tevatron and the LHC ($\mathcal{L} = 100$ pb^{-1}, 14 TeV) for sampled points with $m_a < 2m_\tau$.

cross-section plane. Points with low production cross-section and high branching fraction are nearly singlet ($\mu\kappa/\lambda \ll 60$ GeV) and points with high production cross-section and low branching fraction are nearly doublet ($\mu\kappa/\lambda \gg 60$ GeV). The same limits, presented in the λ, $\mu\kappa/\lambda$ plane, are shown in Fig. 13.

The lightest neutralino in the NMSSM provides a contribution to the cosmological dark matter, and that contribution must be less than or equal to the dark matter density Ω_{DM} from the WMAP 5-year results ($\Omega_{DM} = 0.1099 \pm 0.0062$) [ref]. We used MicrOmegas package [ref], included with NMSSMTools, to compute the NMSSM's dark matter constribution

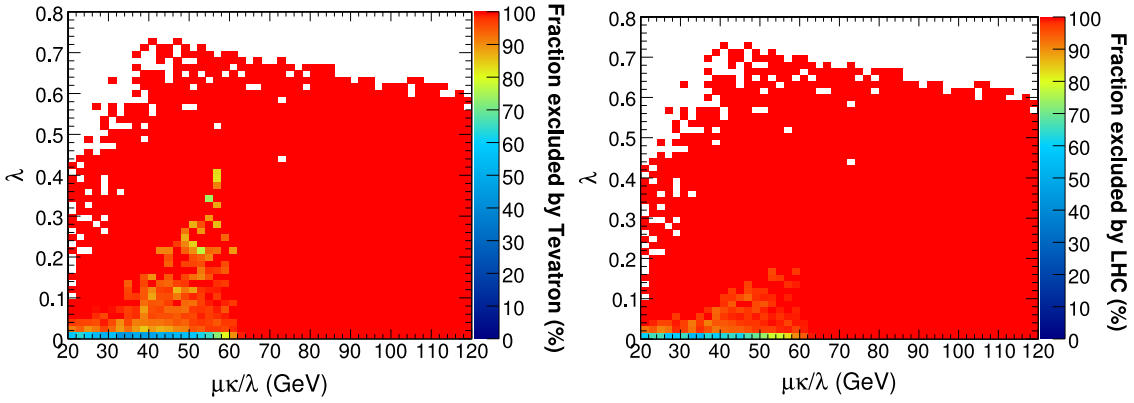

FIG. 13: The fraction of generated models excluded by Tevatron and LHC limits (assuming $\mathcal{L} = 100$ pb^{-1} and 14 TeV: $\sigma(pp \to h_1 \to a_1 a_1 \to 4\mu) < 100$ fb). Red regions are excluded for all values of the other parameters.

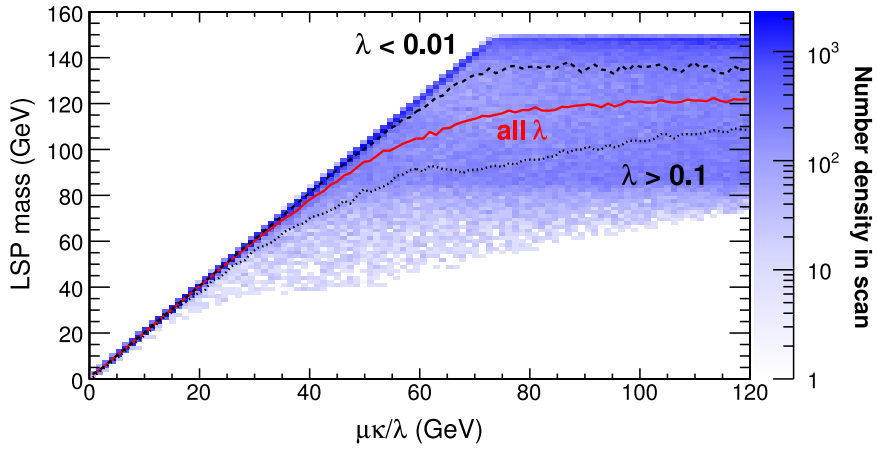

FIG. 14: Mass of the lightest NMSSM neutralino in generated models versus $\mu\kappa/\lambda$ and λ.

Ω_{NMSSM}, selecting $\Omega_{NMSSM} \leq 0.1099 + 2 \times 0.0062$ as a 95% confidence level constraint. Despite the low neutralino masses at small $\mu\kappa/\lambda$ and λ (Fig. 14), this region of parameter space yields large Ω_{NMSSM}, violating the WMAP bound. The cosmological constraint compliments the collider constraint.

To see the fraction of models which survive both constraints, we plot the number of generated models as a function of effective cross-section, coloring the models that have been excluded by the Tevatron and WMAP in Fig. 16. LHC measurements with 100 pb^{-1} of 14 TeV collisions would exclude everything to the right of 0.1 pb (the dashed line). As LHC collisions accumulate, the gap between the region excluded by WMAP and the region

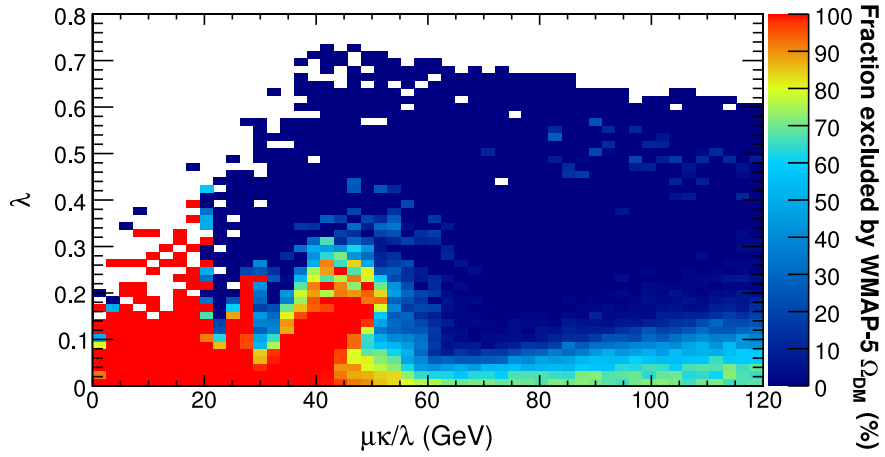

FIG. 15: The fraction of generated models excluded by the WMAP dark matter constraint. Red regions are excluded for all values of the other parameters.

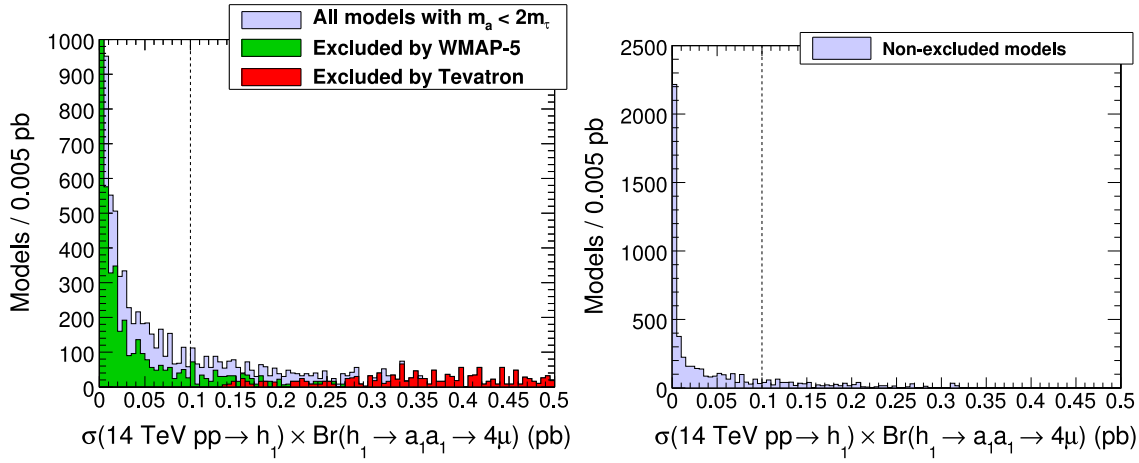

FIG. 16: Left: generated models distributed by their effective LHC cross-section, with excluded models colored. Right: a difference plot, showing only non-excluded models.

excluded by colliders will gradually close.

III. ANALYSIS

The main characteristic of the signal is two back-to-back di-muon pairs with pair consisting of spatially close muons. The di-muon pairs should have invariant masses consistent with each, which serve as a measurement of m_a, and the four muon invariant mass distributionshould have a spike that corresponding to the m_h mass. We use these striking features of signal events in designing the analysis with a reasonably high acceptance and very low

backgrounds suitable for early LHC running.

A. Signal Simulation

We use Pythia to generate signal event templates with m_h in the range from 70 to 140 GeV/c^2 and m_a in the range from 0.5 to 4 GeV/c^2). For detector response emulation, we chose the CMS detector as a benchmark and used its parameters descibed in CMS Technical Design Report. The key parameters important for this analysis are muon momentum resolution, low threshold on muons to reach the muon system, acceptance and average muon reconstruction efficiencies. **we should quote the numbers.**

B. Event Reconstruction

The analysis starts by requiring at least four muon candidates with $p_T > 5$ GeV/$c$in the fiducial volume of the detector. At least one of the four muons has to have $p_T > 20$ GeV/c to suppress major backgrounds and to satisfy trigger requirements. Each event must have at least two muon candidates of positive and negative charge each. In events satisfying these critiria, we define quadruplets of candidates consisting of two positive and two negatively charged muon candidates. Although very unlikely, there can be more than one quadruplet per event, e.g. if there are five muons in the event. Each such quadruplet if preserved until the end of the analysis.

Next, we sort the four muon candidates in quadruplet into two di-muon pairs. We minimize the quantity $(\Delta R(\mu_i, \mu_j)^2 + \Delta R(\mu_k, \mu_l)^2)$ under the constarint that each di-muon pair consists of two muon candidates of opposite charge. We discard quadruplets in which ΔR between muons in any of the two pair exceeds **0.5???** as this cut is 100% efficient for the signal while it can diminish the size of the data sample by removing events, which have topology inconsistent with signal. At his point in the analysis, the invariant mass of each of the di-muon pair, $m_{12}andm_{34}$, is calculated as well as the invariant mass of all four muons, which we denote as m_{1234} or M. Figure 17a) shows the invariant mass of the muon pairs passing all selections (m_{12} and m_{34} are combined into a single distribution) for two choices of m_h and m_a. Figure 17b) shows the distribution of the invariant mass M of the four muon system for two benchmark points. Further background suppression can be

obtained by adding the isolation requirement to one or both di-muon pairs in the event, e.g. by setting the upper bound on the sum of transverse momenta of all tracks in a cone around the reconstructed direction of the di-muon pair excluding momenta of the two muon tracks. Such requirement can allow a very substantial suppression of the dominant source of the background coming from events with one or more muons originating from jets. We choose not to use this critirea as our estimates show that the final rate of such background events is already very low. If data shows larger contribution of these events, this isolation requirement would allow bringing backgrounds back to very low level at a moderate cost to signal acceptance.

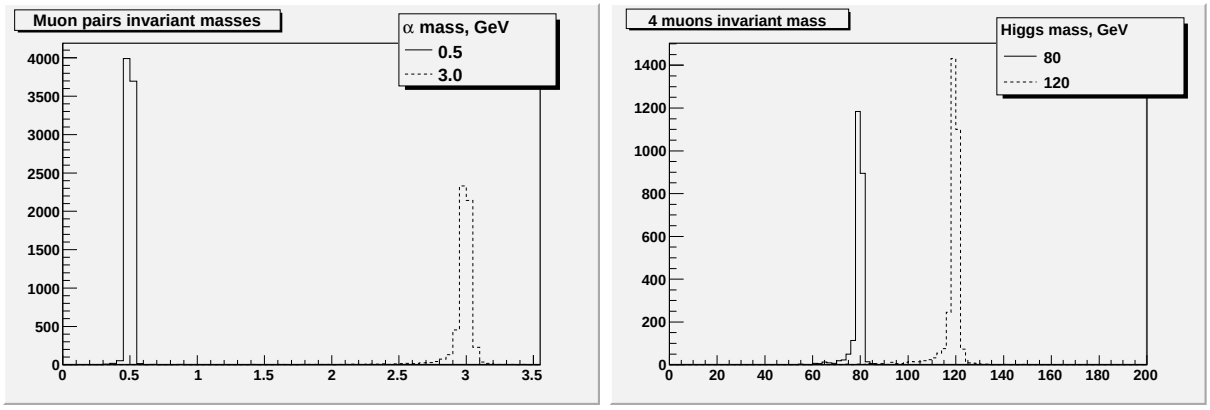

FIG. 17: Left: Reconstructed invariant mass of reconstructed muon pairs for $m_a = 0.5$ and 3 GeV/c^2 (in both cases $m_H = 100$ GeV/c^2). Right: Reconstructed invariant of four muons for $m_H = 80$ and $m_H = 120$ GeV/c^2 (in both cases $m_a = 3.0$ GeV).

Acceptance of the selections listed above is shown in Table I and is large thanks to the high coverage of the CMS muon system. Figures 18a) and 18b) illustrate the dependence of acceptance on values of m_h and m_a.

One can further reduce the background events and zoom on the region of interest of this analysis by applying cuts on m_{12}, m_{34}, M, and require that measured values of m_{12} and m_{34} are consistent within uncertainties. Instead of applying these cuts explicitly, we develop a statistical procedure that performs a fit in a 3D space of measured values of $(m_{12}, m_{34}, m_{1234})$ taking into account kinematical properties of signal events. This approach allows maximizing signal acceptance and therefore statistical power of the analysis and is discussed in what follows. It is also convenient from experimental point of view as the

TABLE I: Acceptances for various points in m_h-m_a space.

m_h, m_a (GeV)	0.5	1.0	2.0	3.0	4.0
80	0.3052 ± 0.0046	0.2656 ± 0.0044	0.2420 ± 0.0043	0.2389 ± 0.0043	0.2324 ± 0.0043
100	0.3915 ± 0.0049	0.3245 ± 0.0047	0.2906 ± 0.0045	0.2862 ± 0.0045	0.2819 ± 0.0045
120	0.4587 ± 0.0050	0.3785 ± 0.0049	0.3405 ± 0.0047	0.3226 ± 0.0047	0.3103 ± 0.0046

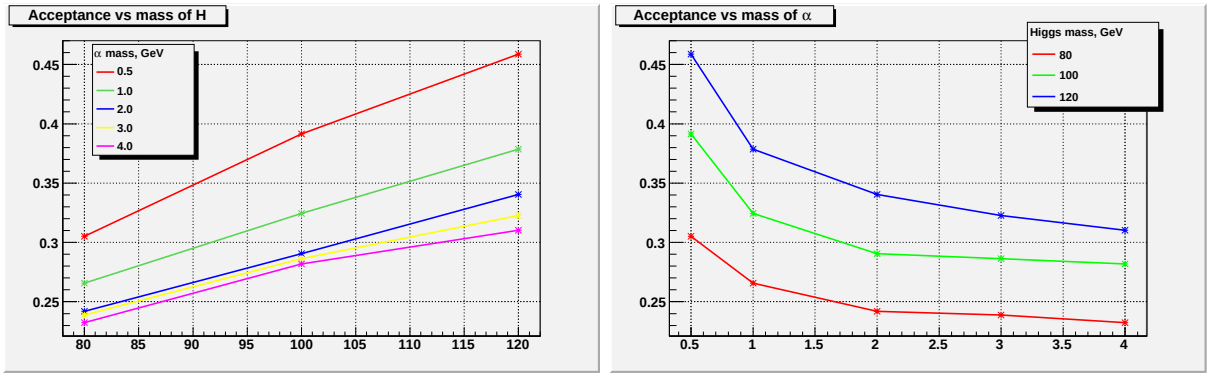

FIG. 18: Acceptance as a function of m_a for fixed m_h. Acceptance as a function of m_h for fixed m_a.

backgrounds will be distributed in some smooth fashion over the 3D space allowing fitting the 3D distribution to estimate backgrounds directly from the data. Potential signal would appear as a concentration of events in one specific region in the 3D space (a 3D "bump"). Figure 19 shows the difference in the reconstructed masses of the two di-muon pairs in signal events, which determines the size of the signal region in the (m_{12}, m_{34}) plane.

To give the reader a better idea on the signal significance of this analysis, we quote efficiencies and background contamination (next section) for a set of cuts that zooms on the highest significance region. The cuts we use are $M > 60$ GeV/c^2, $m_{12} < 4$, $m_{34} < 4$, and $|m_{12} - m_{34}| < 0.08 + 0.005 * (m_{12} + m_{34})$. The latter cut is enforcing the requirement that the two pair masses are consistent with each other and takes into account widening of the absolute resolution in the reconstructed di-muon mass as a function of mass.

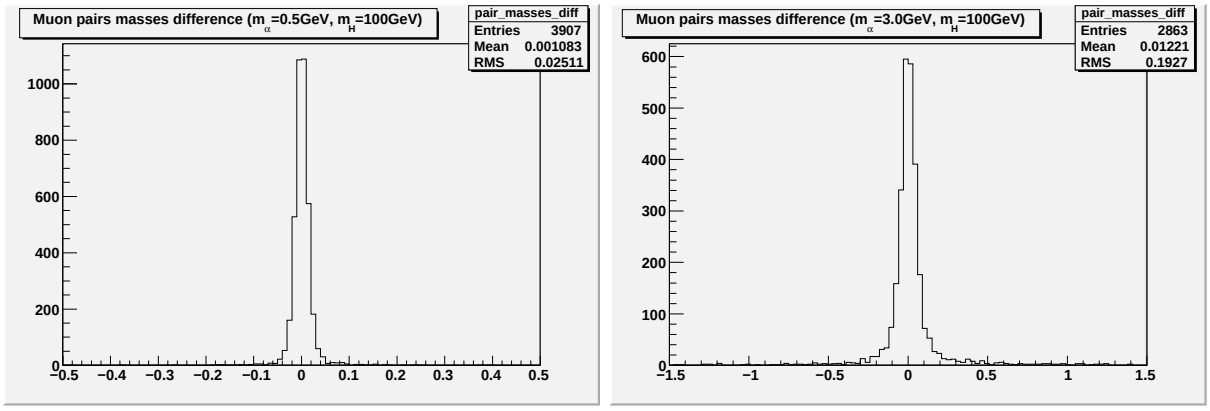

FIG. 19: Left: Muon pairs masses difference (m_a=0.5GeV, m_H=100 GeV). Right: Muon pairs masses difference (m_a=3.0GeV, m_H=100 GeV)

C. Background Estimation

The main backgrounds in this analysis are QCD multijet events where muons originate from either heavy flavor quark decays or from K/π decays in flight. We also considered electroweak backgrounds and direct J/psi production, but found those contributions completely negligible. Requirement of four sufficiently energetic muons in the event drastically reduces contributions of all background processes. Further constarints on the correlation of di-muon pair masses and relatively high invariant mass of the four muon system allows an essentially zero background analysis. In the following we discuss estimation of these backgrounds.

1. QCD backgrounds

The largest contribution comes from rare QCD multi-jet events with four energetic reconstructed muons that are produced either in heavy flavor decays of b and c mesons (real muons) or in K/π decays in flight. The punch-through contamination is heavily suppresed due to massive shileding of the CMS muon system. The multi-jet background is drastically reduced by the requirement of at least one muon with $p_T > 20$ GeV/c and the follow up selections. Background events surviving selections can be divided into two fractions: events with all four real muons from heavy flavor meson decays and events with typically three real muons and a misidentified muon from K/π decays in flight. The first source is estimated using Pythia MC 2→2 QCD jet production by selecting generated muons and smearing dis-

tributions using detector resolutions and efficiencies. The second contamination is estimated using the same Pythia sample by selecting events with two or three real muons and one or more charged pions or kaons satisfying p_T and η requirements used for muons. Each such event is assigned a weight calculated as the probability that available K/π mesons decay into muons before reaching radius of $\simeq$2 meters (**halfway into the hadronic calorimeter - is it what we want?**). We find that the level of backgrounds due to misidentifications is comparable to the rate of the backgrounds associated with real muons from heavy flavor decays. While the fraction of remaining events after acceptance cuts does not appear negligible, these events are spread over the 3D space with only a tiny fraction of them appearing in the region where signal would appear, see Tables III and V. If necessary, these remaining backgrounds can be completely eliminated by applying a loose track isolation requirement on one of both of the di-muon pairs.

2. Electroweak four lepton backgrounds

We use CompHEP to generate a large sample of events with four muons in final state coming from the electroweak processes. The cross-section of this process is 0.5 pb (Sasha, is this correct? Kind of sounds very small!!!) and after a cut on the first muon $p_T > 20$ GeV/c, the large chunk of remaining events are $Z\gamma^*$ type events. Very few of these events have muons that can be arranged into pairs with low invariant mass, and the fraction of events with similar masses of the pairs is completely negligible.

3. Other SM Backgrounds

We also studied several other processes, e.g. direct J/ψ production process that can produce a pair of muons with mass in the range of interest of this analysis and another pair of muons can come from decays in flight. We used Pythia MC and a weighing technique similar to the QCD case and find that this background is completely negligible. Other SM backgrounds (top, W+jets) are negligible in the region of interest of this analysis.

TABLE II: Background cuts efficiency for generator level

Cuts	4 leptons	$\mu + x$	J/Ψ
1st eta<2.4	0.7994 ± 0.0040	0.95638 ± 0.00073	0.0088 ± 0.0022
2nd eta<2.4	0.8295 ± 0.0042	0.99992 ± 0.00003	$1.00^{+0.00}_{-0.06}$
3rd eta<2.4	0.8541 ± 0.0044	0.99584 ± 0.00024	0.75 ± 0.11
4th eta<2.4	0.7066 ± 0.0061	0.96407 ± 0.00068	0.75 ± 0.13
1st pt>5	0.9805 ± 0.0022	$1.00000^{+0}_{-0.00001}$	$1.0^{+0.0}_{-0.1}$
2nd pt>5	0.9405 ± 0.0038	0.8676 ± 0.0013	$1.0^{+0.0}_{-0.1}$
3rd pt>5	0.7893 ± 0.0068	0.0445 ± 0.0008	0.3333 ± 0.1571
4th pt>5	0.4390 ± 0.0093	0.0284 ± 0.0032	$0.00^{+0.27}_{-0.00}$
1st pt>20	0.9524 ± 0.0060	0.9873 ± 0.0126	0
analysis acceptance	0.1218 ± 0.0033	0.00099 ± 0.00011	0
pair masses<4	0.0025 ± 0.0014	0.3333 ± 0.0533	0
inv. mass>60	0.6667 ± 0.3333	0.4231 ± 0.0969	0
$\lvert m_{12} - m_{34} \rvert < 0.08$			
$+0.005 * (m_{12} + m_{34})$	$X.XXXX \pm X.XXXX$	$X.XXXX \pm X.XXXX$	0
full efficiency	0.000203 ± 0.000143	0.00014 ± 0.00004	0

4. Summary

While the number of background events past the acceptance stage and that are used in the fit is not small, the fitting procedure described in the next section is effectively reducing the region of interest to events that have kinematic properties of signal events making backgrounds nearly completely negligible, as illustarted by the lower part of Table V showing the number of expected background events after each cut in a dataset corresponding to 100 $\text{pb}^{-1}$of LHC data. **We need a plot to show background distributions, e.g. m12 and m1234 - we have them, just need to clean up**.

TABLE III: Background cuts efficiency for reco level

Cuts	4 leptons	$\mu + x$	J/Ψ
1st pt>5	0.7455 ± 0.0044	$1.00000^{+0}_{-0.00001}$	$1.0000^{+0}_{-0.0006}$
2nd pt>5	0.7012 ± 0.0053	$1.00000^{+0}_{-0.00001}$	$1.0000^{+0}_{-0.0006}$
3rd pt>5	0.6066 ± 0.0068	0.04349 ± 0.0007	0.3333 ± 0.0013
4th pt>5	0.3300 ± 0.0084	0.0402 ± 0.0034	$0.00^{+0.15}_{-0.00}$
1st pt>20	0.9573 ± 0.0063	$1.000^{+0}_{-0.007}$	0
analysis acceptance	0.1002 ± 0.0030	0.0017 ± 0.0002	0
pair masses<4	0.0041 ± 0.0020	0.3358 ± 0.0403	0
inv. mass>60	0.50 ± 0.25	0.4348 ± 0.0731	0
$\lvert m_{12} - m_{34}\rvert < 0.08$ GeV			
$+0.005 * (m_{12} + m_{34})$	$X.XXXX \pm X.XXXX$	$X.XXXX \pm X.XXXX$	0
full efficiency	0.00020 ± 0.00014	0.00025 ± 0.00006	0

IV. STATISTICAL ANALYSIS OF THE DATA

To maximize sensitivity and emulate real data analysis techniques, we define a likelihood function in the 3D space ($m_{pair\,1}$, $m_{pair\,2}, M$), where M is the four muon invariant mass. The likelihood is defined as follows:

$$\mathcal{L}(m_h, m_a, \sigma(pp{\rightarrow}h)) = \prod_i \mathcal{P}(\sigma(pp{\rightarrow}h)\ L\ BR_{h\rightarrow aa} BR^2_{a\rightarrow\mu\mu} L\alpha(m_h, m_a) N_i^S(m_a, m_h) + L\ N_i^B, N_i^D) \quad (6)$$

where i runs over bins in 3D space of $(m_{12}, m_{34}, m_{1234})$, m_h is the light higgs mass, m_a is axial higgs mass, $\mathcal{P}(\nu, N)$ is Poisson probability for observing N events when the true rate is ν. Other parameters are dataset luminosity L, acceptance of the signal events $\alpha(m_h, m_a)$, N_i^S is the fraction of reconstructed signal events in bin i ($\Sigma N_i^S = 1$), N_i^B is the rate of background events in bin i per unit of luminosity.

Because of the limited statistics in the Monte Carlo samples describing QCD backgrounds, we parameterize the background distriution in the (m_{12}, m_{34}, M) space using the following

TABLE IV: Expected number of background events after each selection cut on generator level

Cuts	4 leptons	Incl. muon	JPsi
Initial number	48.21 ± 0.49	152878.11 ± 546.06	120.91 ± 2.84
1st eta<2.4	38.54 ± 0.43	146209.61 ± 534.01	1.0652 ± 0.2663
2nd eta<2.4	31.97 ± 0.40	146197.91 ± 533.99	1.0652 ± 0.2663
3rd eta<2.4	27.30 ± 0.37	145589.38 ± 532.88	0.7989 ± 0.2306
4th eta<2.4	19.29 ± 0.31	140358.34 ± 523.22	0.5992 ± 0.1997
1st pt>5	18.92 ± 0.30	140358.34 ± 523.22	0.5992 ± 0.1997
2nd pt>5	17.79 ± 0.30	121774.70 ± 487.35	0.5992 ± 0.1997
3rd pt>5	14.04 ± 0.26	5424.13 ± 102.86	0.1997 ± 0.1153
4th pt>5	6.17 ± 0.17	154.08 ± 17.34	$0^{+0.067}_{-0.000}$
1st pt>20	5.87 ± 0.17	152.13 ± 17.23	$--$
pair masses<4	0.0147 ± 0.0085	50.71 ± 9.95	$--$
inv. mass>60	0.0098 ± 0.0069	21.45 ± 6.47	$--$
$\lvert m_{12} - m_{34} \rvert < 0.08$ GeV			
$+0.005 * (m_{12} + m_{34})$	$0.000^{+0.005}_{-0.000}$	$0.00^{+1.95}_{-0.00}$ **??**	$--$

function:

$$B(m_{12}, m_{34}, m_{1234}) = f(m_{12}) \times f(m_{34}) \times g(m_{1234}) \tag{7}$$

$$f(m_{12}) = \tag{8}$$

$$g(m_{1234}) =, \tag{9}$$

This simple function describes backgrounds very well in the region of interest because typical four muon invariant mass values are much larger than the narrow range of di-muon pair masses effectively leading to very little correlation of the two. An important note is that using this parameterization requires that in the data analysis the order of pairs has to be randomized (e.g. designating m_{12} to be the mass of the pair that contains highest p_T muon will break factorization), and so we randomize them in the analysis. Fitted parameters of the function are shown in Table **??**. We verified that background events found in MC are well described by this function by running pseudoexperiments using paramaterized distribution

TABLE V: Expected number of background events after each selection cut on reco level

Cuts	4 leptons	Incl. muon	JPsi
Initial number	48.21 ± 0.49	152878.11 ± 546.06	120.91 ± 2.84
1st pt>5	35.94 ± 0.42	152878.11 ± 546.06	120.91 ± 2.84
2nd pt>5	21.20 ± 0.35	152878.11 ± 546.06	0.3995 ± 0.1631
3rd pt>5	15.29 ± 0.27	6648.99 ± 113.88	$0^{+0.067}_{-0.000}$
4th pt>5	5.04 ± 0.16	267.21 ± 22.83	$--$
1st pt>20	4.83 ± 0.15	267.21 ± 22.83	$--$
pair masses<4	0.0049 ± 0.0098	89.72 ± 13.23	$--$
inv. mass>60	0.0098 ± 0.0069	39.01 ± 8.72	$--$
$\lvert m_{12} - m_{34}\rvert < 0.08$ GeV			
$+0.005 * (m_{12} + m_{34})$	$0.000^{+0.005}_{-0.000}$	$0.00^{+1.95}_{-0.00}$ **??**	$--$

and verifying that the p-value for the outcome similar to what is observed in MC is high.

Thus defined likelihood function can be used to calculate the 95% C.L. upper limit on the cross-section times branching ratio of the $h \to \mu\mu\mu\mu$ signal or determine the intergrated luminosity required to make a discovery at a certain level. These results can then be translated into the exclusion region in (m_a, m_h) parameter space or NMSSM parameter space. To demonstrate performance of this technique, Figures 20a) and b) show calculated likelihood functions for two pseudoexperiments, in one of which no signal was injected into the pseudodata and in the other a certain amount of signal was admixed in addition to background contributions. In both cases, likelihood function shows expected behavior.

We calculate the 95% C.L. upper limit on the product $\sigma(pp \to h) B_{h \to aa} B^2_{a \to \mu\mu}\, \alpha$, using Bayesian technique which is 0.0293 pb at $L = 100$ pb^{-1}, approximately 3 events. In vast majority of pseudoexperiments, this limit is independent of m_h and m_a because the effective signal region that dominates signal significance in the fitter is essentially background free and probability to observe any pseudodata event is very small. Since $B_{a \to \mu\mu}$ is nearly a function of m_a only, it can be factored out, and the corresponding upper limit on $\sigma(pp \to h) B_{h \to aa} \alpha$ is presented in Table VI. The upper limit on $\sigma(pp \to h) B_{h \to aa}$ is shown as a function of m_h and m_a in Table VII by factoring out α as well. Keep in mind that $B_{h \to aa}$ is close to 100%

in much of our preferred region of NMSSM parameter space.

TABLE VI: 95% C.L. on $\sigma(pp\to h)B_{h\to aa}\,\alpha$ at $L = 100$ pb^{-1} as a function of m_a, from Fig **??**.

m_a (GeV)	$B_{a\to\mu\mu}$ (%)	$\sigma(pp\to h)B_{h\to aa}\,\alpha$ (pb)
0.5	0	∞
0.75	4.2	16.5
1.0	10.0	2.9
1.5	15.7	1.2
2.0	17.2	1.0
2.5	17.1	1.0
3.0	16.1	1.1
3.5	14.8	1.3
3.75	1.02	282
4.0	0.73	557
5.0	0.49	1220

TABLE VII: 95% C.L. on $\sigma(pp\to h)B_{h\to aa}$ (pb) at $L = 100$ pb^{-1}, from Fig **??** and Table I.

m_h, m_a (GeV)	0.5	1.0	2.0	3.0	4.0
80	∞	10.9	4.1	4.6	2400
100	∞	8.9	3.4	3.8	2000
120	∞	7.7	2.9	3.4	1800

V. RESULTS

TO BE WRITTEN

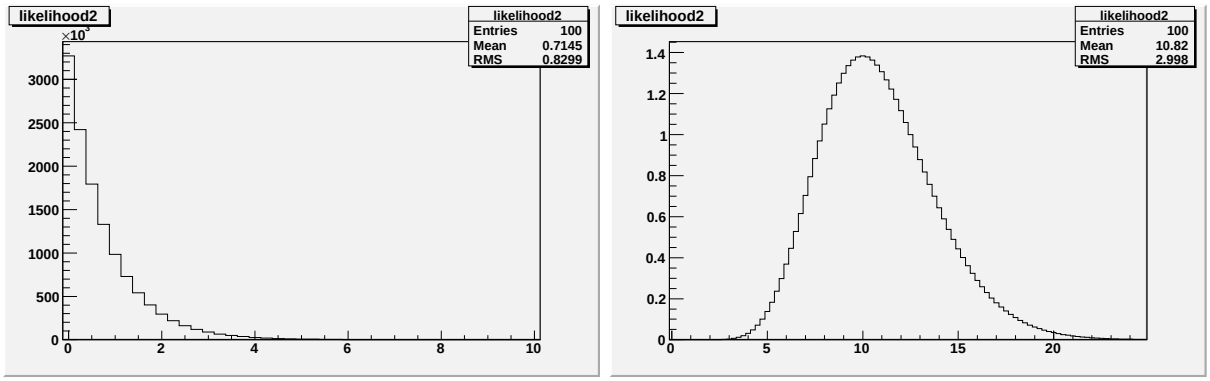

FIG. 20: Left:Example likelihood for a pseudoexperiment for a search assuming $B(H\to aa\to\mu\mu\mu\mu)$=0.04, m_a = 3 GeV, m_h = 100 GeV with null signal shows that a 95% exclusion is somewhere around 2.5 pb for $\sigma(pp\to H)$. Right: Example likelihood for $\sigma(pp\to H)$=10 pb^{-1}, $B(H\to aa\to\mu\mu\mu\mu)$=0.04, m_a = 3 GeV m_h = 100 GeV shows a more than 5σ observation.

Acknowledgments

We thank XXX and YYY

[1] H. P. Nilles, M. Srednicki and D. Wyler, Phys. Lett. B **120** (1983) 346.
[2] J. M. Frere, D. R. T. Jones and S. Raby, Nucl. Phys. B **222** (1983) 11.
[3] J. R. Ellis, J. F. Gunion, H. E. Haber, L. Roszkowski and F. Zwirner, Phys. Rev. D **39** (1989) 844.
[4] M. Drees, Int. J. Mod. Phys. A **4** (1989) 3635.
[5] U. Ellwanger, Phys. Lett. B **303** (1993) 271 [arXiv:hep-ph/9302224].
[6] U. Ellwanger, M. Rausch de Traubenberg and C. A. Savoy, Phys. Lett. B **315** (1993) 331 [arXiv:hep-ph/9307322].
[7] T. Elliott, S. F. King and P. L. White, Phys. Rev. D **49** 2435 (1994) 2435 [arXiv:hep-ph/9308309].
[8] P. N. Pandita, Z. Phys. C **59** (1993) 575.
[9] U. Ellwanger, M. Rausch de Traubenberg and C. A. Savoy, Z. Phys. C **67** (1995) 665 [arXiv:hep-ph/9502206].
[10] S. F. King and P. L. White, Phys. Rev. D **52** (1995) 4183 [arXiv:hep-ph/9505326].
[11] F. Franke and H. Fraas, Int. J. Mod. Phys. A **12** (1997) 479 [arXiv:hep-ph/9512366].
[12] U. Ellwanger, M. Rausch de Traubenberg and C. A. Savoy, Nucl. Phys. B **492** (1997) 21 [arXiv:hep-ph/9611251].
[13] D. J. Miller, R. Nevzorov and P. M. Zerwas, Nucl. Phys. B **681** (2004) 3.
[14] J. E. Kim and H. P. Nilles, Phys. Lett. B **138**, 150 (1984).
[15] R. Dermisek and J. F. Gunion, Phys. Rev. Lett. **95**, 041801 (2005) [arXiv:hep-ph/0502105].

[16] B. A. Dobrescu, G. L. Landsberg and K. T. Matchev, Phys. Rev. D **63**, 075003 (2001) [arXiv:hep-ph/0005308]; B. A. Dobrescu and K. T. Matchev, JHEP **0009**, 031 (2000) [arXiv:hep-ph/0008192].

[17] J. F. Gunion, H. E. Haber and T. Moroi, *In the Proceedings of 1996 DPF / DPB Summer Study on New Directions for High-Energy Physics (Snowmass 96), Snowmass, Colorado, 25 Jun - 12 Jul 1996, pp LTH095* [arXiv:hep-ph/9610337]; U. Ellwanger, J. F. Gunion and C. Hugonie, arXiv:hep-ph/0111179

[18] J. R. Ellis, J. F. Gunion, H. E. Haber, L. Roszkowski and F. Zwirner, Phys. Rev. D **39**, 844 (1989); B. A. Dobrescu, G. L. Landsberg and K. T. Matchev, Phys. Rev. D **63**, 075003 (2001) [arXiv:hep-ph/0005308];
U. Ellwanger, J. F. Gunion, C. Hugonie and S. Moretti, arXiv:hep-ph/0305109; U. Ellwanger, J. F. Gunion, C. Hugonie and S. Moretti, arXiv:hep-ph/0401228; U. Ellwanger, J. F. Gunion and C. Hugonie, JHEP **0507**, 041 (2005) [arXiv:hep-ph/0503203].

[19] S. Moretti, S. Munir and P. Poulose, Phys. Lett. B **644**, 241 (2007) [arXiv:hep-ph/0608233];

[20] S. Chang, P. J. Fox and N. Weiner, Phys. Rev. Lett. **98**, 111802 (2007) [arXiv:hep-ph/0608310].

[21] R. Dermisek and J. F. Gunion, Phys. Rev. D **75**, 075019 (2007) [arXiv:hep-ph/0611142].

[22] K. Cheung, J. Song and Q. S. Yan, Phys. Rev. Lett. **99**, 031801 (2007) [arXiv:hep-ph/0703149].

[23] J. R. Forshaw, J. F. Gunion, L. Hodgkinson, A. Papaefstathiou and A. D. Pilkington, JHEP **0804** (2008) 090 [arXiv:0712.3510 [hep-ph]].

[24] A. Belyaev, S. Hesselbach, S. Lehti, S. Moretti, A. Nikitenko and C. H. Shepherd-Themistocleous, arXiv:0805.3505 [hep-ph].

[25] A. Menon, D. E. Morrissey and C. E. M. Wagner, Phys. Rev. D **70** (2004) 035005 [arXiv:hep-ph/0404184]; D. G. Cerdeno, C. Hugonie, D. E. Lopez-Fogliani, C. Munoz and A. M. Teixeira, JHEP **0412** (2004) 048 [arXiv:hep-ph/0408102]; G. Belanger, F. Boudjema, C. Hugonie, A. Pukhov and A. Semenov, JCAP **0509**, 001 (2005) [arXiv:hep-ph/0505142]; J. F. Gunion, D. Hooper and B. McElrath, Phys. Rev. D **73**, 015011 (2006) [arXiv:hep-ph/0509024]; F. Ferrer, L. M. Krauss and S. Profumo, Phys. Rev. D **74**, 115007 (2006) [arXiv:hep-ph/0609257]; D. G. Cerdeno, E. Gabrielli, D. E. Lopez-Fogliani, C. Munoz and A. M. Teixeira, JCAP **0706**, 008 (2007) [arXiv:hep-ph/0701271]; C. Hugonie, G. Belanger and A. Pukhov, JCAP **0711**, 009 (2007) [arXiv:0707.0628 [hep-ph]]; V. Barger, P. Langacker, I. Lewis, M. McCaskey, G. Shaughnessy and B. Yencho, Phys. Rev. D **75**, 115002 (2007) [arXiv:hep-ph/0702036]. S. Kraml, A. R. Raklev and M. J. White, Phys. Lett. B **672**, 361 (2009) [arXiv:0811.0011 [hep-ph]]; G. Belanger, C. Hugonie and A. Pukhov, JCAP **0901**, 023 (2009) [arXiv:0811.3224 [hep-ph]].

[26] U. Ellwanger, J.F. Gunion and C. Hugoine, JHEP **0502**, 066 (2005).

[27] U. Ellwanger, C. Hugoine, Comput. Phys. Commun. **175**, 290 (2006).

[28] F. Domingo and U. Ellwanger, arXiv:0710.3714 [hep-ph].

[29] G. Abbiendi *et al.* (OPAL Collaboration), Eur. Phys. J. C **18**, 425-445 (2001).

[30] G. Abbiendi *et al.* (OPAL Collaboration), Eur. Phys. J. C **27**, 483-495 (2003), arXiv:0209068v1 [hep-ex].

[31] M. Spira, A. Djouadi, D. Graudenz and P. M. Zerwas, Nucl. Phys. B **453**, 17 (1995) [arXiv:hep-ph/9504378].

[32] A. Djouadi, J. Kalinowski and M. Spira, Comput. Phys. Commun. **108**, 56 (1998) [arXiv:hep-ph/9704448].

[33] C. Balazs, H. J. He and C. P. Yuan, Phys. Rev. D **60**, 114001 (1999) [arXiv:hep-ph/9812263].

[34] A. Belyaev, J. Pumplin, W. K. Tung and C. P. Yuan, JHEP **0601**, 069 (2006) [arXiv:hep-

TABLE VIII: Background samples normalization

Sample	σ	N_{evt}^{gen}	Filter efficiency	L_{eff}	$f = L_{100}/L_{eff}$
$\mu + x$	$0.5091mb$	6238383	0.000239	$51.2709pb^{-1}$	1.9504
4 leptons	$0.538pb$	10995	1.0	$20436.803pb^{-1}$	0.0049
J/ψ	$0.127.2nb$	1413803	0.0074	$1502.00pb^{-1}$	0.0666

ph/0508222].

VI. APPENDIX